Photoionization of *N*-Alkylphenothiazines in Mesoporous Metal Silicoaluminophosphate Molecular Sieves

Jae Young Bae, Koodali T. Ranjit, Zhaohua Luan, R. M. Krishna, and Larry Kevan*

Department of Chemistry, University of Houston, Houston, Texas 77204-5641

Received: April 19, 2000; In Final Form: August 8, 2000

The photoionization of *N*-alkylphenothiazines (PC_n where $n = 1$, 3, 6, 10, and 16) in mesoporous silicoaluminophosphate (UHM-3) and transition metal-substituted silicoaluminophosphate (MUHM-3 where M = Cu, Ni, Cr, and Mn) molecular sieves has been studied by electron spin resonance with ultraviolet irradiation at room temperature. Mesoporous UHM-3 and MUHM-3 molecular sieves were synthesized at room temperature. The effect of the ratio of Si/Al, the nature of the transition metal, and the concentration of the metal on the photoyield was examined. *N*-Alkylphenothiazine was incorporated into these mesoporous materials and the photoionization of PC_n was studied.

Introduction

Photoionization of molecules in heterogeneous systems[1−4] such as vesicles and micelles,[5−17] colloidal solutions,[18−20] zeolites (molecular sieves),[21−27] and silica gels[28−39] has been used as model systems for light energy storage. The design of efficient artifical photoredox systems[1−4] for photochemical energy conversion and storage must prevent rapid back electron transfer[40−42] to achieve long-lived photoinduced charge separation. Heterogeneous systems[22−27] have been found to be better hosts than homogeneous systems for such photoredox systems.

N-Alkylphenothiazines with longer alkyl chains are excellent photoactive electron donors. They can be easily oxidized by ultraviolet (UV) irradiation to form *N*-alkylphenothiazine cation radicals, which have been characterized by electron spin resonance (ESR) and optical spectroscopic techniques.[43−50] Grätzel et al. used flash photolysis to study the photooxidation of phenothiazine and methylphenothiazine in micelles.[15,51−53] Hovey used steady-state photolysis and ESR at room temperature to study the air photooxidation of methylphenothiazine in micelles.[54] Photoactive electron donors such as *N*-alkylphenothiazines can be incorporated inside heterogeneous hosts, and such heterogeneous hosts can stabilize photoinduced radical cations with relative ease.[55,56]

Researchers at Mobil Corporation synthesized silica-based mesoporous M41S molecular sieve materials[57−59] in 1992. Zhao et al.[60−63] reported the successful formation of mesoporous hexagonal aluminophosphate (UHM-1) and silicoaluminophosphate (UHM-3) molecular sieves as heterogeneous hosts by a modified ion-pair process. These molecular sieves show a regular hexagonal array of uniform tubes with a diameter of about 3.5 nm, a high surface area of about 850 m^2/g, and a pore size distribution nearly as sharp as that of zeolites.

In the present research, mesoporous hexagonal UHM-3 and metal-substituted UHM-3 (MUHM-3 where M = Cu, Ni, Cr, and Mn) molecular sieves have been synthesized by using optimum mixture and stirring conditions at room temperature to improve the thermal stability and are used as heterogeneous hosts for long-lived photoinduced electron transfer from *N*-alkylphenothiazines PC_n where $n = 1$, 3, 6, 10, and 16 (Figure 1). The photoionization of PC_n in UHM-3 and MUHM-3 molecular sieves has been studied by ESR after UV irradiation at room temperature. The photoyield was found to depend on the Si/Al ratio, the nature of the transition metal ion, the M/Al ratio, and the alkyl chain length of PC_n.

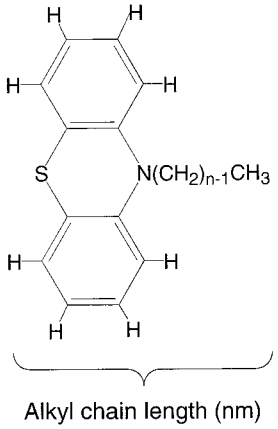

PC_n	Alkyl chain length (nm)
1	0.6
3	0.8
6	1.1
10	1.4
16	2.0

Figure 1. Structure of *N*-Alkylphenothiazines.

Experimental Section

Synthesis of UHM-3 and CuUHM-3. We have improved the syntheses of hexagonal mesostructured silicoaluminophosphate (UHM-3) and hexagonal mesostructured copper-substituted silicoaluminophosphate (CuUHM-3) molecular sieves to increase the thermal stability (calcined at 700 °C) by varying the mixture composition and the stirring speed. Copper-substituted silicoaluminophosphate (CuUHM-3) molecular sieves possess reasonable thermal stability and high specific surface area by modifying the synthetic conditions reported by Zhao et al.[61] for manganese-substituted aluminophosphate-based mesoporous molecular sieve. It has been shown that incorporation of transition metal ions into microporous aluminophosphate successfully improves its Bronsted acidity and increases the potential of these materials as catalysts.[64−67]

Mesoporous hexagonal silicoaluminophosphate (UHM-3) molecular sieves were synthesized according to Zhao et al.[60−63] by using cetyltrimethylammonium chloride (CTACl, Aldrich,

* Author to whom correspondence should be addressed.

10.1021/jp001500h CCC: $19.00
Published on Web 09/26/2000

25% in water) as a structure-directing agent and aluminum hydroxide (53.5 wt % Al_2O_3, USP Pfaltz & Bauer Inc.), phosphoric acid (85 wt %, EM Industries), and tetraethyl orthosilicate (TEOS, Aldrich) as aluminum, phosphorus, and silicon sources, respectively, at room temperature. Optimization for the best synthetic conditions gives P/Al of 1.00, CTACl/Al of 0.8, slow stirring (300 rpm) and pH 9.0.

Copper-containing mesoporous hexagonal silicoaluminophosphate (CuUHM-3) molecular sieves were synthesized by using a similar procedure with 0.1 M $CuCl_2$ (Aldrich) added into the silicoaluminophosphate gel with stirring before the addition of the CTACl surfactant solution. The composition of the resultant gel was Al_2O_3:P_2O_5:(0.4−2.4)SiO_2:(1×10^{-3}−1)$CuCl_2$:0.8CTACl:(8−9)TMAOH:(455−550)H_2O. The organic structure-directing agent in the pores of these gels was removed by calcination at 700 °C for 2 h in flowing nitrogen, followed by 12 h in flowing oxygen.

Synthesis of the *N*-Alkylphenothiazines (PC_n where n = 1, 3, 6, 10, and 16). Commercial methylphenothiazine (PC_1, Aldrich) was used as received. Four *N*-alkylphenothiazines (PC_n where n = 3, 6, 10, and 16) were synthesized.[68] During the purification of PC_n we used ethyl acetate instead of methylisobutyl ketone as used earlier. The synthetic details for propylphenothiazine (PC_3), *N*-hexylphenothiazine (PC_6), decylphenothiazine (PC_{10}), and hexadecylphenothiazine (PC_{16}) are as follows.

Ten grams (for PC_3), 12 g (for PC_6), or 15 g (for PC_{10} or PC_{16}) of phenothiazine (Aldrich, 98%) was dissolved in 250 mL (for PC_3), 300 mL (for PC_6), or 350 mL (for PC_{10} or PC_{16}) of anhydrous tetrahydrofuran, and 2.5 g (for PC_3), 3.0 g (for PC_6), or 3.5 g (for PC_{10} or PC_{16}) of sodium hydride (Aldrich) was added to the solution slowly while the solution was stirred, respectively. The reaction system was kept under nitrogen. After the solution was stirred for 4 h (for PC_3), 8 h (for PC_6), or 10 h (for PC_{10} or PC_{16}) at room temperature, 10 g (for PC_3) of 1-bromopropane (Aldrich, 99+%), 14 g (for PC_6) of 1-bromohexane (Aldrich, 98%), 18 g (for PC_{10} or PC_{16}) of 1-bromodecane (Aldrich, 98%) or 1-bromohexadecane (Aldrich, 97%) was added, and the solution was refluxed at room temperature for 48 h, respectively. The progress of the reaction was monitored with thin-layer chromatography. When all of the phenothiazine was consumed, the reaction was quenched by pouring the solution into a separatory funnel, followed by the addition of 100 mL of water and 100 mL of ethyl acetate. The organic layer was separated and the aqueous layer was washed with ethyl acetate. The combined organic extracts were washed with water, and the remaining solvent was concentrated by evaporation under reduced pressure. The resulting crude products were purified by liquid chromatography (Aldrich silica gel, 60−200 mesh, *n*-hexane eluant). The compounds were identified by NMR spectroscopy. The ^{1}H NMR of PC_3 in $CDCl_3$ showed absorption peaks at 1.05 (CH_3), 1.92 (CH_2CN), 3.94 (CH_2N), and 6.94−7.45 ppm (phenothiazine ring protons). The ^{1}H NMR of PC_6 in $CDCl_3$ showed absorption peaks at 1.03 (CH_3), 1.10−1.60 ($C(CH_2)_3C$), 1.90−1.93 (CH_2CN), 3.91 (CH_2N), and 6.94−7.56 ppm (phenothiazine ring protons). The ^{1}H NMR of PC_{10} in $CDCl_3$ showed absorption peaks at 1.03 (CH_3), 1.38−1.42 ($C(CH_2)_7C$), 1.95 (CH_2CN), 3.55 (CH_2N), and 6.97−7.29 ppm (phenothiazine ring protons). The ^{1}H NMR of PC_{16} in $CDCl_3$ showed absorption peaks at 0.91 (CH_3), 1.12−1.64 ($C(CH_2)_{13}C$), 1.86 (CH_2CN), 3.41 (CH_2N), and 6.85−7.25 ppm (phenothiazine ring protons).

Preparation of Samples and Measurements. Metal ions were incorporated into the UHM-3 materials in both extraframework and framework positions. To incorporate metal ions into extraframework positions, ion exchange of protons in the calcined H-UHM-3 materials was done by liquid-state ion exchange. Typical liquid-state ion exchange was performed by adding 2 mL of 1×10^{-3} M $CuCl_2 \cdot 2H_2O$, $NiCl_2 \cdot 6H_2O$, $MnCl_2 \cdot 4H_2O$, or $CrCl_3 \cdot 6H_2O$, and 18 mL of water to 0.2 g of H-UHM-3 and the mixture was stirred overnight at room temperature. The samples were then filtered, washed with warm distilled water to remove any excess metal ions on the surface of the sample, and then dried in air to form MH-UHM-3.

Incorporation of the *N*-alkylphenothiazines into UHM-3 was performed by impregnation. For impregnation, 0.1 g of UHM-3 was put into 1 mL of 1×10^{-2} M *N*-alkylphenothiazine in benzene for overnight in the dark. The benzene was removed by flowing nitrogen gas over the sample for 30 min. For ESR measurements the same amount of the sample was transferred into Suprasil quartz tubes (2 mm i.d. × 3 mm o.d.) which were sealed at one end.

Powder X-ray diffraction (XRD) patterns of all UHM-3 and MUHM-3 samples were obtained on a Philips 1840 powder diffractometer with Cu Kα radiation (40 kV, 25 mA) at 0.01° step width and 1 s step time over the range $1.5° < 2\theta < 10°$. The samples were mounted on aluminum slides in order to avoid preferential ordering. Chemical analysis was performed by electron microprobe analysis on a JEOL JXA-8600 spectrometer. The composition of all UHM-3 and MUHM-3 materials was determined by calibration with known standards and by averaging over several defocused areas to give the bulk composition. Thermogravimetric analysis (TGA) of all UHM-3 and MUHM-3 materials was performed on a TGA 2050 analyzer from TA Instruments with a heating rate of 10 °C min^{-1} in oxygen. N_2 adsorption isotherms were measured at 77 K using a Micromeritics Gemini 2375 analyzer. The volume of adsorbed N_2 of all UHM-3 and MUHM-3 materials was normalized to standard temperature and pressure. Prior to experiments, samples were dehydrated at 250 °C for 3 h. The BET specific surface area was determined from the linear part of the BET equation (P/P_o = 0.05−0.31). The calculation of the pore size distribution was performed using the desorption branches of the N_2 adsorption isotherms and the Barrett−Joyner−Halenda (BJH) formula.[69] Although the BJH analysis underestimates the pore size,[70−73] relative changes in the pore size should be accurately portrayed. The cumulative mesopore (1.7−10.0 nm) surface area, A_{BJH}, was obtained from the pore size distribution curves. The ESR spectra were recorded at room temperature at 9.5 GHz using a Bruker ESP 300 spectrometer with 100 kHz field modulation and low microwave power to avoid power saturation. Photoproduced *N*-alkylphenothiazine cation radicals (PC_n^+) yields were determined by double integration of the ESR spectra using the ESP 300 software. Each photoyield is an average of three determinations.

The PC_n/UHM-3 materials were irradiated using a 300 W Cermax Xenon lamp (ILC-LX 300 UV) at room temperature. The incoming light was passed through a 10 cm water filter to prevent infrared radiation and through a Corning No. 7-54 filter to filter light of wavelengths shorter than 320 nm. The samples were placed in a quartz Dewar and rotated at a speed of 4 rpm to ensure even irradiation.

Results

Powder XRD patterns of as-synthesized and calcined UHM-3 and CuUHM-3 are shown in Figure 2. Well-defined XRD patterns show a prominent peak at 2.3° 2θ and some broad but clearly present peaks in the 2θ range of 3.0°−6.0°. As-

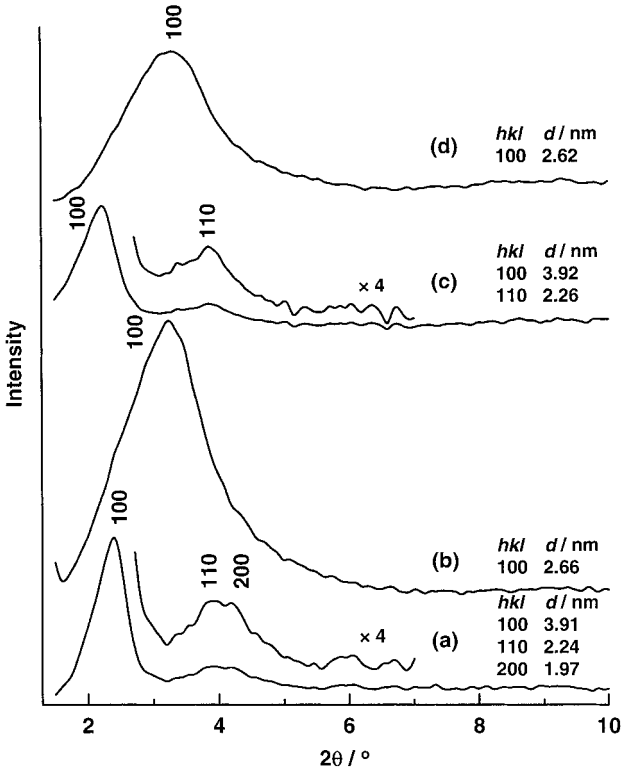

Figure 2. Powder XRD patterns of (a) as-synthesized UHM-3 (Si/Al = 0.4), (b) calcined UHM-3 (Si/Al = 0.4), (c) as-synthesized CuUHM-3 (Si/Al = 0.4 and Cu/Al = 0.1), and (d) calcined CuUHM-3 (Si/Al = 0.4 and Cu/Al = 0.1).

synthesized UHM-3 and CuUHM-3 show a $d(100)$ spacing of 3.9 nm and a unit cell parameter ($a_o = 2d(100)/3^{1/2}$)[74−82] of 4.5 nm. The integrity of the mesoporous structures of UHM-3 and CuUHM-3 is retained even after complete decomposition of the organic structure-directing agent by calcination at 700 °C in flowing nitrogen for 2 h, followed by 12 h in flowing oxygen. All XRD patterns of calcined UHM-3 and CuUHM-3 are similar and exhibit a single broad diffraction peak corresponding to a $d(100)$ spacing of 2.6 nm and a unit cell parameter of 3.0 nm. The broadening of the $d(100)$ reflection on calcination arises from less long-range crystallographic order. The $d(100)$ peaks shift from 3.9 to 2.6 nm for calcined UHM-3 and CuUHM-3. The pore structure of these materials is believed to be a three-dimensional, disordered network of short, wormlike, tubular channels, while the channel widths are uniform.

TGA of UHM-3 shows a large weight loss of 70% on heating to 700 °C. Three endothermic losses near 70 °C (15% weight loss), 230 °C (25% weight loss), and 300 °C (30% weight loss) are observed. The 70 °C weight loss is assigned to water desorption. The 230 °C and 300 °C weight losses are assigned to desorption and decomposition of TMAOH and CTACl in either order. CuUHM-3 shows a similar TGA curve as UHM-3.

Figure 3 shows typical N_2 adsorption isotherms from calcined UHM-3 and CuUHM-3 samples. Both give typical irreversible type I behavior as defined by IUPAC,[83] indicating the presence of micropores. Calcined UHM-3 had a BET surface area of 829 $m^2\ g^{-1}$ and an average pore diameter of 1.7 nm. Calcined CuUHM-3 had a BET surface area of 1248 $m^2\ g^{-1}$ and an average pore diameter of 1.7 nm, which suggests that incorporation of copper can improve the thermal stability. These results indicate the presence of tubular microporous and mesoporous mixed-channels in UHM-3 and CuUHM-3 materials. The

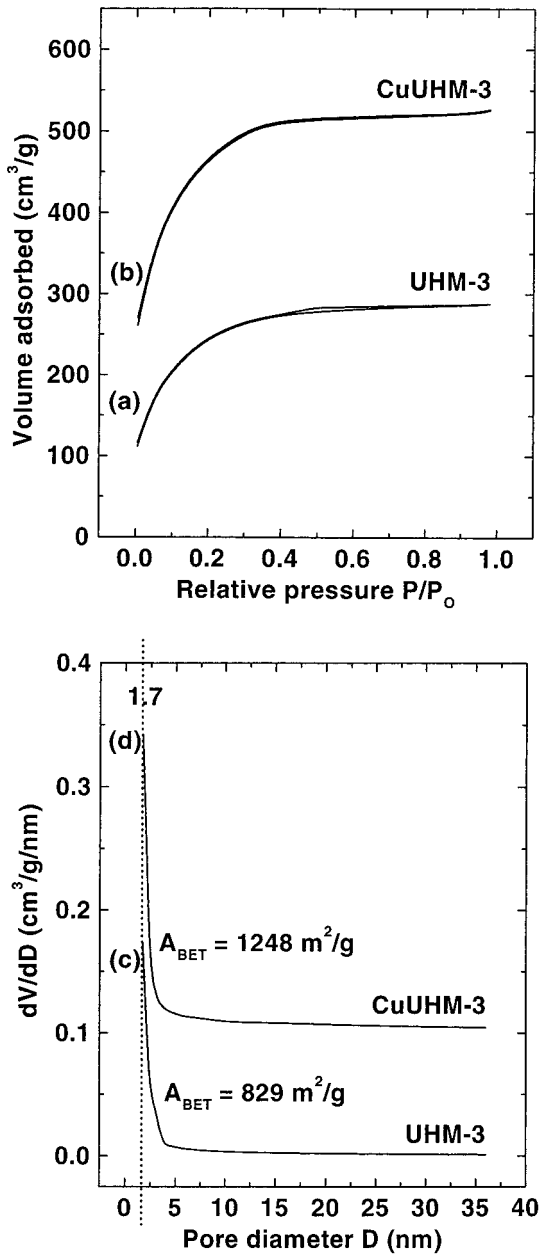

Figure 3. Adsorption−desorption isotherms of nitrogen at 77 K for (a) calcined UHM-3 (Si/Al = 0.4) and (b) calcined CuUHM-3 (Si/Al = 0.4 and Cu/Al = 0.1). Corrresponding pore size distribution curves for (c) calcined UHM-3 (Si/Al = 0.4) and (d) calcined CuUHM-3 (Si/Al = 0.4 and Cu/Al = 0.1).

approximate pore size calculation by nitrogen physisorption is smaller than the repeat distance $a_o = 3.0$ nm determined by XRD ($a_o = 2d(100)/3^{1/2}$, where $d(100) = 2.6$ nm), because the latter includes the thickness of the pore wall. Thus, we can estimate that the pore walls of these UHM-3 and CuUHM-3 materials are about 1.3 nm thick.

For calcined M-UHM-3 samples (M = Cu, Ni, Cr) ESR results show that Cu and Ni are in the +2 oxidation state and that Cr is in the +3 oxidation state.

The photoionization of PC_n in the synthesized mesoporous molecular sieves was examined. The effects of the Si/Al ratio, the nature of the transition metal, the metal concentration, and the alkyl chain length on the photoyield were examined. The photoyields of samples evacuated to remove traces of water or solvent were similar to those of unevacuated samples so the possible influence of such adsorbed impurities seems negligible.

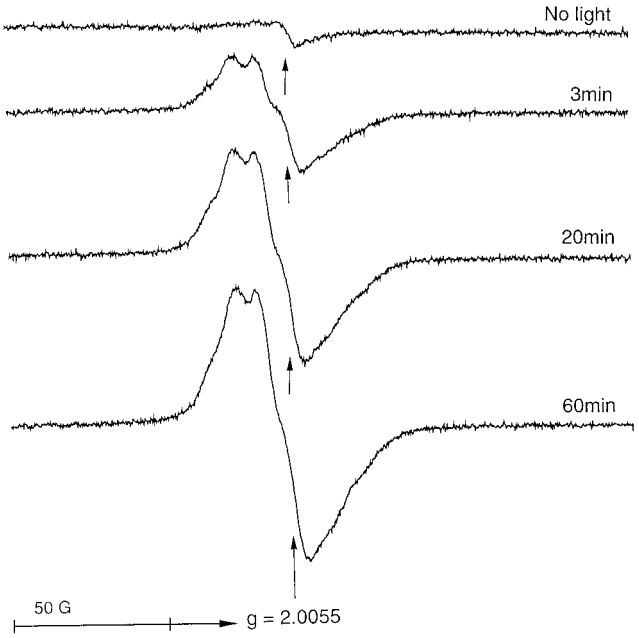

Figure 4. ESR spectra of PC_1/UHM-3 (Si/Al = 0.4) versus photoirradiation time.

The samples with methylphenothiazine introduced into UHM-3 (Si/Al = 0.4) show only weak ESR signals before irradiation (Figure 4). This indicates that some methylphenothiazine cation radicals are generated during the sample preparation process. After being irradiated by 320 nm light at room temperature for 3 min, the samples show strong ESR signals. With further increase in irradiation time to 20 min, the intensity of the ESR signal increases further and then almost reaches a plateau after 60 min. This shows that a substantial number of stable radicals are produced by the irradiation. These ESR spectra are broad, partially resolved, and asymmetric. The spectral widths of Figure 4, which show the ESR spectra of samples containing PC_1, are the same as those of the methylphenothiazine cation radicals in homogeneous solution and in micelles at room temperature.[45,54] The ESR spectra observed before irradiation have the same line shape as those observed after irradiation although they are much weaker. PC_1-impregnated commercial silica gel samples, PC_1/IP2.5, PC_1/IP4.0, and PC_1/IP1.7,[35] show the same ESR signal as in this sample after 20 min room-temperature irradiation. The impregnated samples are colorless before irradiation and turn pink after irradiation.

Figure 5 shows the increase in the ESR signal intensities of PC_1-containing samples PC_1/UHM-3 (Si/Al = n) with n = 0.4, 0.8, 1.2, and 2.4 with irradiation time. From Figure 5 it is seen that the highest photoyield is obtained for PC_1/UHM-3 (Si/Al = 0.4). The ESR signals increase rapidly during the first 20 min and then almost reach a plateau. An irradiation time of 60 min was selected for comparative photoyield and decay studies. The rate of formation of the PC_1^+ cation radicals can be evaluated from the initial slope in Figure 5 assuming first-order kinetics. The calculated rate constants for the formation of PC_1^+ cation radicals are $k = 380 \times 10^{-4}$ s^{-1} for PC_1/UHM-3 (Si/Al = 0.4), $k = 87 \times 10^{-4}$ s^{-1} for PC_1/UHM-3 (Si/Al = 0.8), and $k = 27 \times 10^{-4}$ s^{-1} for PC_1/UHM-3 (Si/Al = 1.2 and 2.4). The photoyield of the photoproduced PC_1^+ cation radicals was evaluated and it was found that PC_1/UHM-3 (Si/Al = 0.4) exhibited the highest photoyield toward PC_1^+ cation radicals. The decay of the photoproduced PC_1^+ cation radicals as monitored by ESR is also an important factor in the design of efficient photoredox systems. In the case of PC_1/UHM-3 (Si/Al = n) with n = 0.4, 0.8, 1.2, and 2.4, the ESR intensity was essentially the same for several hours. Hence, for all these samples, the intensity of the ESR signal was monitored every 24 h. The half-life times ($t_{1/2}$) for PC_1/UHM-3 (Si/Al = n) with n = 0.4, 0.8, 1.2, and 2.4 were estimated to be $t_{1/2}$ = 3 days for Si/Al = 0.4, $t_{1/2}$ = 5 days for Si/Al = 0.8, $t_{1/2}$ = 52 days for Si/Al = 1.2, and $t_{1/2}$ = 93 days for Si/Al = 2.4. The stability of the photoproduced PC_1^+ cation radicals was evaluated, and it was found that PC_1/UHM-3 (Si/Al = 2.4) exhibited the highest stability toward PC_1^+ cation radicals.

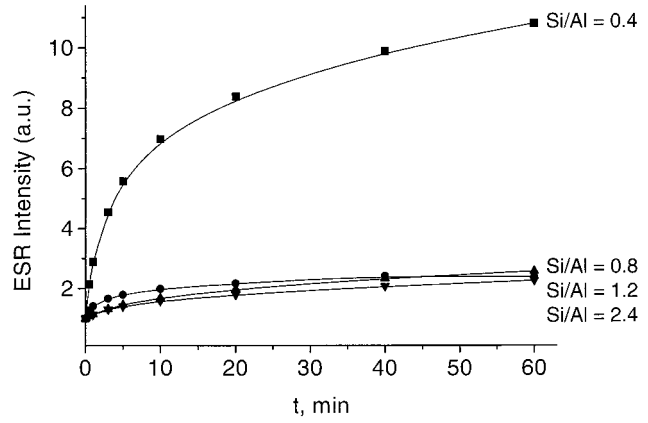

Figure 5. Increase of ESR intensities at room temperature of PC_1/UHM-3 (Si/Al = n) (where n = 0.4, 0.8, 1.2, and 2.4) versus photoirradiation time.

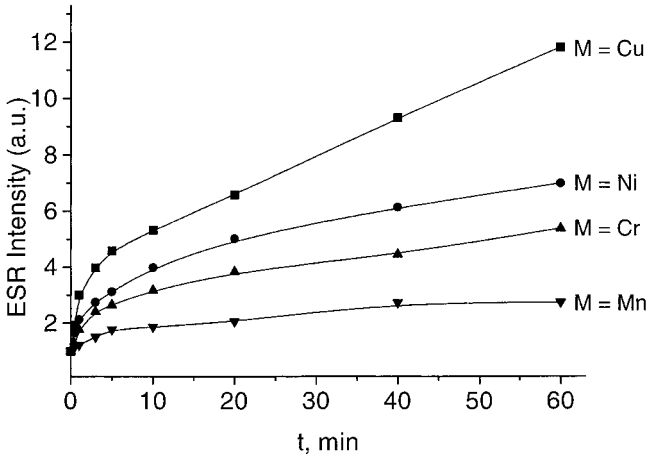

Figure 6. Increase of ESR intensities at room temperature of PC_1/MH-UHM-3 (Si/Al = 0.4) (where M = Cu, Ni, Cr, and Mn) at room temperature versus photoirradiation time.

Figure 6 shows the increase in the ESR signal intensities of PC_1-containing samples PC_1/MH-UHM-3 (Si/Al = 0.4) with M = Cu, Ni, Cr, and Mn with irradiation time. From Figure 6 it is seen that the highest photoyield is obtained for PC_1/CuH-UHM-3 (Si/Al = 0.4). The calculated rate constants for the formation of PC_1^+ cation radicals are $k = 290 \times 10^{-4}$ s^{-1} for PC_1/CuH-UHM-3 (Si/Al = 0.4), $k = 218 \times 10^{-4}$ s^{-1} for PC_1/NiH-UHM-3 (Si/Al = 0.4), $k = 148 \times 10^{-4}$ s^{-1} for PC_1/CrH-UHM-3 (Si/Al = 0.4), and $k = 57 \times 10^{-4}$ s^{-1} for PC_1/MnH-UHM-3 (Si/Al = 0.4). The photoyield of the photoproduced PC_1^+ cation radicals was evaluated and it was found that PC_1/CuH-UHM-3 (Si/Al = 0.4) exhibited the highest photoyield toward PC_1^+ cation radicals. In the case of decay of PC_1/MH-UHM-3 (Si/Al = 0.4) with M = Cu, Ni, Cr, and Mn the ESR intensity was essentially the same for several hours. The half-life times ($t_{1/2}$) for PC_1/MH-UHM-3 (Si/Al = 0.4) with M = Cu, Ni, Cr, and Mn were estimated to be $t_{1/2}$ = 22 days for M

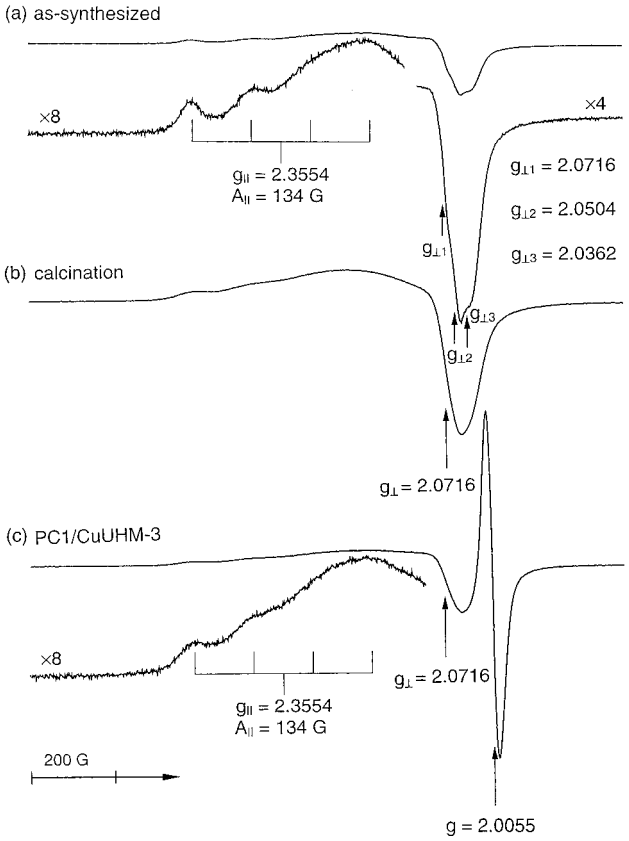

Figure 7. ESR spectra at room temperature of (a) as-synthesized CuUHM-3 (Si/Al = 0.4 and Cu/Al = 0.1), (b) calcined CuUHM-3 (Si/Al = 0.4 and Cu/Al = 0.1) in O_2 at 700 °C for 12 h, and (c) PC_1/CuUHM-3 (Si/Al = 0.4 and Cu/Al = 0.1).

= Cu, $t_{1/2}$ = 4 days for M = Ni, $t_{1/2}$ = 3 days for M = Cr, and $t_{1/2}$ = 2 days for M = Mn. The stability of the photoproduced PC_1^+ cation radicals was evaluated and it was found that PC_1/CuH-UHM-3 (Si/Al = 0.4) exhibited the highest stability toward PC_1^+ cation radicals.

Figure 7 shows ESR spectra of (a) as-synthesized CuUHM-3 (Si/Al = 0.4 and Cu/Al = 0.1), (b) calcined CuUHM-3 in O_2 at 700 °C for 12 h, and (c) PC_1-containing samples PC_1/CuUHM-3. The powder ESR spectrum of as-synthesized CuUHM-3 can be described by an axial **g** tensor with $g_{||}$ = 2.3554, $g_{\perp1}$ = 2.0716, $g_{\perp2}$ = 2.0504, $g_{\perp3}$ = 2.0362, and an axial metal ion hyperfine coupling with $A_{||} = 147 \times 10^{-4}$ cm^{-1}. The Cu(II) hyperfine coupling in the perpendicular part of the powder spectrum was not resolved. In copper-substituted CuUHM-3 the $g_{\perp}$ values are assigned to the three different environments, one inside, another outside and another one on the hexagonal tubular walls, respectively. The powder ESR spectrum of calcined CuUHM-3 shows a single Cu(II) species described by $g_{||}$ = 2.3554, $g_{\perp}$ = 2.0716, and $A_{||} = 147 \times 10^{-4}$ cm^{-1}. The observation of only $g_{\perp}$ = 2.0716 ($g_{\perp1}$ value of as-synthesized CuUHM-3) indicates that after calcination metal ions are only present on the hexagonal tubular walls. The spin Hamiltonian parameters for PC_1/CuUHM-3 are the same as for calcined CuUHM-3 with g = 2.0055 for PC_1^+.

Figure 8 shows the increase in the ESR signal intensities of PC_1-containing samples PC_1/CuUHM-3 (Si/Al = 0.4 and Cu/Al = n) with $n = 1 \times 10^{-3}$, 1×10^{-2}, 1×10^{-1}, and 1 with irradiation time. The photoyield is also dependent on the amount of metal content in the UHM-3 materials. From Figure 8 it is seen that the highest photoyield is obtained for PC_1/CuUHM-3 (Si/Al = 0.4 and Cu/Al = 1×10^{-3}). The calculated rate

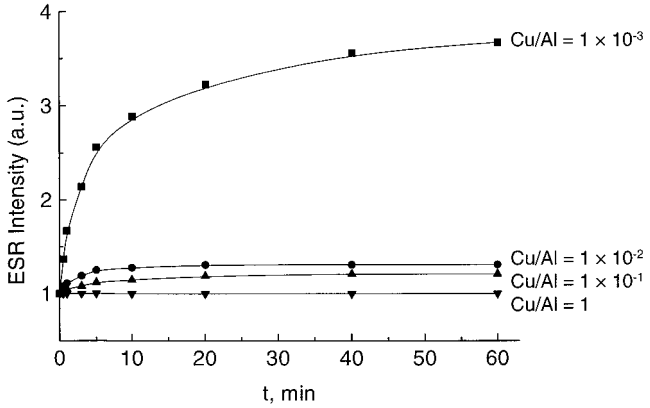

Figure 8. Increase of ESR intensities at room temperature of PC_1/CuUHM-3 (Si/Al = 0.4 and Cu/Al = n) (where $n = 1 \times 10^{-3}$, 1×10^{-2}, 1×10^{-1}, and 1) at room temperature versus photoirradiation time.

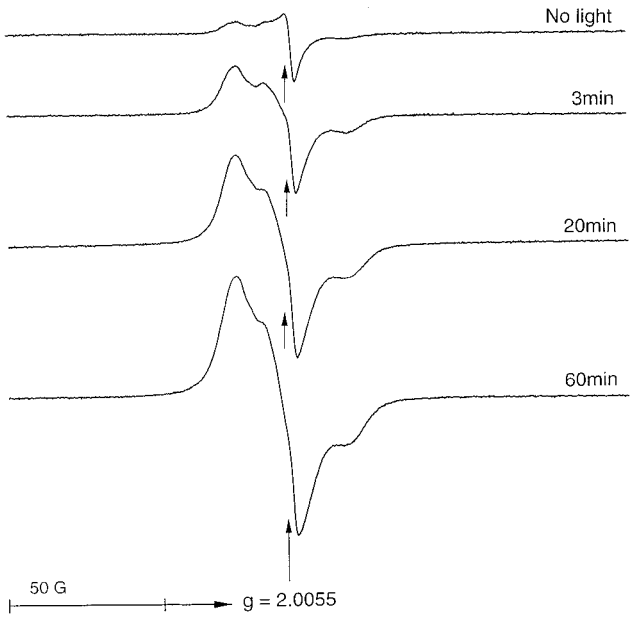

Figure 9. ESR spectra at room temperature of PC_{10}/UHM-3 (Si/Al = 2.4) versus photoirradiation time.

constants for the formation of PC_1^+ cation radicals are $k = 123 \times 10^{-4}$ s^{-1} for PC_1/CuUHM-3 (Si/Al = 0.4 and Cu/Al = 1×10^{-3}), $k = 27 \times 10^{-4}$ s^{-1} for PC_1/CuUHM-3 (Si/Al = 0.4 and Cu/Al = 1×10^{-2}), and $k = 3 \times 10^{-4}$ s^{-1} for PC_1/CuUHM-3 (Si/Al = 0.4 and Cu/Al = 1×10^{-1} or 1). The photoyield of the photoproduced PC_1^+ cation radicals was evaluated and it was found that PC_1/CuUHM-3 (Si/Al = 0.4 and Cu/Al = 1×10^{-3}) exhibited the highest photoyield toward PC_1^+ cation radicals. In the case of decay of PC_1/CuUHM-3 (Si/Al = 0.4 and Cu/Al = n) with $n = 1 \times 10^{-3}$, 1×10^{-2}, 1×10^{-1}, and 1, the ESR intensity was essentially the same for several days. The half-life times ($t_{1/2}$) for PC_1/CuUHM-3 (Si/Al = 0.4 and Cu/Al = n) with $n = 1 \times 10^{-3}$, 1×10^{-2}, 1×10^{-1}, and 1 were estimated to be $t_{1/2}$ = 23 days for Cu/Al = 1×10^{-3}, $t_{1/2}$ = 20 days for Cu/Al = 1×10^{-2}, $t_{1/2}$ = 14 days for Cu/Al = 1×10^{-1}, and 1. The stability of the photoproduced PC_1^+ cation radicals was evaluated and it was found that PC_1/CuUHM-3 (Si/Al = 0.4 and Cu/Al = 1×10^{-3}) exhibited the highest stability toward PC_1^+ cation radicals.

The sample PC_{10}/UHM-3 (Si/Al = 2.4) shows only weak ESR signals before irradiation (Figure 9). This indicates that some decylphenothiazine cation radicals are generated during the

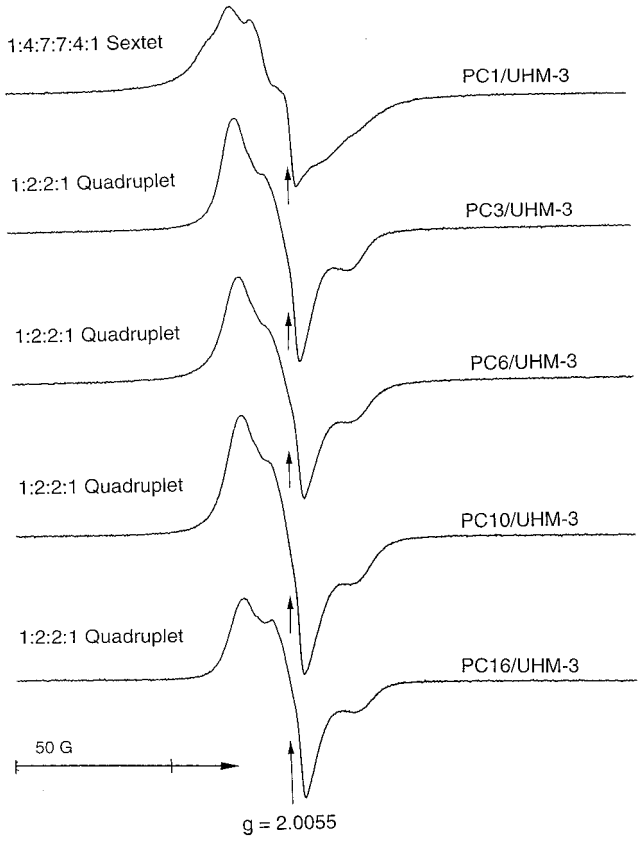

Figure 10. ESR spectra at room temperature of PC_n/UHM-3 (Si/Al = 2.4) (where n = 1, 3, 6, 10, and 16) samples after 60 min room temperature irradiation at 320 nm.

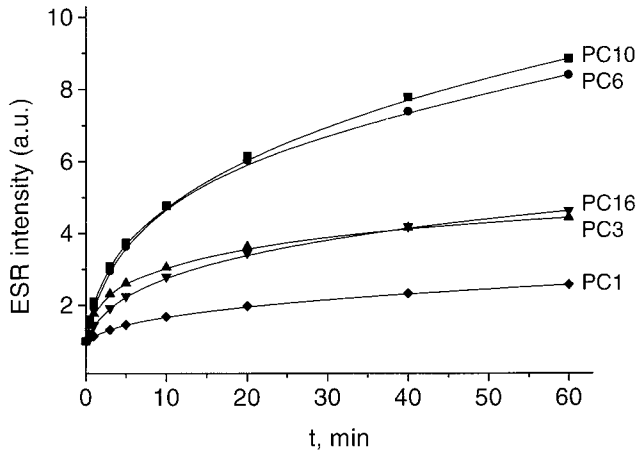

Figure 11. Increase of ESR intensities at room temperature of PC_n/UHM-3 (Si/Al = 2.4) (where n = 1, 3, 6, 10, and 16) versus photoirradiation time.

sample preparation process. The samples with decylphenothiazine introduced into PC_n/UHM-3 (Si/Al = 2.4) (where n = 1, 3, 6, 10, and 16) show strong ESR signals after 60 min room-temperature irradiation at 320 nm (Figure 10).

Figure 11 shows the increase in the ESR signal intensities of PC_n-containing samples PC_n/UHM-3 (Si/Al = 2.4) with n = 1, 3, 6, 10, and 16 with irradiation time. From Figure 11 it is seen that the highest photoyield is obtained for PC_{10}/UHM-3 (Si/Al = 2.4). The calculated rate constants for the formation of PC_n^+ cation radicals are $k = 203 \times 10^{-4}$ s^{-1} for PC_{10}/UHM-3 (Si/Al = 2.4), $k = 170 \times 10^{-4}$ s^{-1} for PC_6/UHM-3 (Si/Al = 2.4), $k = 143 \times 10^{-4}$ s^{-1} for PC_{16}/UHM-3 (Si/Al = 2.4), $k = 77 \times 10^{-4}$ s^{-1} for PC_3/UHM-3 (Si/Al = 2.4), and $k = 27 \times 10^{-4}$ s^{-1}

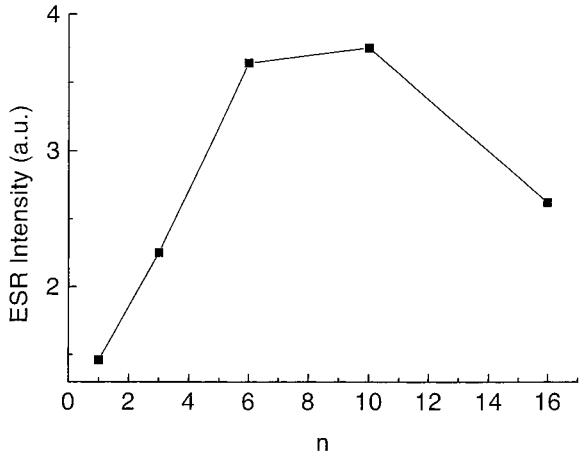

Figure 12. Room-temperature photoyields based on ESR intensities of PC_n/UHM3 (Si/Al = 2.4) (where n = 1, 3, 6, 10, and 16) measured after 60 min photoirradiation at room temperature versus the alkyl chain length of the *N*-alkylphenothiazines.

for PC_1/UHM-3 (Si/Al = 2.4). The photoyield of the photoproduced PC_n^+ cation radicals was evaluated and it was found that PC_{10}/UHM-3 (Si/Al = 2.4) exhibited the highest photoyield toward PC_{10}^+ cation radicals. In the case of decay of PC_n/UHM-3 (Si/Al = 2.4) with n = 1, 3, 6, 10, and 16 the ESR intensity was essentially the same for several days. The half-life times ($t_{1/2}$) for PC_n/UHM-3 (Si/Al = 2.4) with n = 1, 3, 6, 10, and 16 were estimated to be $t_{1/2}$ = 150 days for PC_{10} and PC_6, $t_{1/2}$ = 114 days for PC_3, $t_{1/2}$ = 93 days for PC_1, and $t_{1/2}$ = 32 days for PC_{16}. The stability of the photoproduced PC_n^+ cation radicals was evaluated and it was found that PC_{10}/UHM-3 (Si/Al = 2.4) and PC_6/UHM-3 (Si/Al = 2.4) exhibited the highest stability toward PC_{10}^+ and PC_6^+ cation radicals. The net photoionization yields of PC_n/UHM-3 (Si/Al = 2.4) are plotted as a function of the pendent alkyl chain length in Figure 12. An irradiation time of 60 min was selected for comparative yields.

Discussion

Improved thermal stability of mesoporous UHM-3 and CuUHM-3 molecular sieves was obtained by the modified synthesis to survive calcination at 700 °C with an average pore diameter of 1.7 nm and a 1.3 nm thick pore wall (Figures 2 and 3). The photoionization of *N*-alkylphenothiazines with alkyl chain lengths of 0.6−2.0 nm (Figure 1) was studied for these materials.

A little dark reaction occurs during sample preparation. This is not completely understood although it is not uncommon in oxide materials. Defect sites in UHM-3 or residual light exposure may produce some oxidation of PC_1. However, the photooxidation of PC_1 is much greater than any thermal oxidation.

To understand the influence of the Si/Al ratio on the photoyield, several mesoporous UHM-3 molecular sieves were prepared. The strong ESR signals of PC_1^+ cation radicals in PC_1/UHM-3 (Si/Al = 0.4) after irradiation by 320 nm at room temperature in Figure 4 show a sextet with g = 2.0055. The hyperfine structure depends on the interaction of the unpaired electron with nitrogen and protons. The ESR spectrum of PC_1^+ cation radicals exhibits a sextet with relative intensities of 1:4:7:7:4:1 showing interaction with nitrogen and three protons of a methyl group.[84−87]

The ESR spectra of PC_1^+ cation radicals photoproduced at room temperature in PC_1/UHM-3 with different Si/Al ratios have

the same line shapes as that of chemically produced PC_1^+ cation radicals in UHM-3 with Si/Al = 0.4. But the intensities of the photoproduced PC_1^+ cation radicals vary with different Si/Al ratios (Figure 5). The ESR signal intensities of PC_1^+ cation radicals of Figure 5 clearly confirm the photooxidation of methylphenothiazine molecules into PC_1^+ cation radicals in UHM-3 with different Si/Al ratios by 320 nm irradiation at room temperature. The UHM-3 framework is the likely electron acceptor. Surface hydroxyl groups may serve as electron acceptors at low Si/Al ratio with production of a hydrogen atom. However, this seems relatively inefficient since the photoionization yields are small for high Si/Al ratio. Mesoporous UHM-3 molecular sieves of low Si/Al ratio possess more surface hydroxyl groups than UHM-3 molecular sieves of high Si/Al ratio because the surface hydroxyl groups are bonded to aluminums. The photoyield increases as the Si/Al ratio decreases.

To understand the influence of metal type, various metal ion-exchanged mesoporous MH-UHM-3 molecular sieves were prepared with a Si/Al ratio of 0.4. The variable valence metal ions can act as electron acceptors. Experiments with transition metal ions (Cu, Ni, Cr, and Mn) in mesoporous UHM-3 show strong ESR signals at room temperature. Figure 6 shows the increase in the intensities of the ESR signals due to PC_1^+ cation radicals with irradiation time for MH-UHM-3, with transition metal ions in ion-exchange sites. As one can observe from Figure 6, the presence of Cu in mesoporous UHM-3 enhances the photoyield more compared to Ni, Cr, and Mn. The photoionization efficiency of transition metal ions in UHM-3 decreases in the order, CuH-UHM-3 > NiH-UHM-3 > CrH-UHM-3 > MnH-UHM-3. Thus the photoionization efficiency can be controlled by the nature of the metal ion in ion-exchange sites.

The higher photoyield and stability of the methylphenothiazine cation radicals can be accounted for on the basis of higher electron affinity of Cu^{2+} ($E°$ $Cu^{2+}/Cu^{1+} = 0.153$) as compared to Cr^{3+} ($E°$ $Cr^{3+}/Cr^{2+} = -0.407$) and Mn^{2+} ($E°$ $Mn^{2+}/Mn^{1+} = -3.0$) and of Cu^{2+} ($E°$ $Cu^{2+}/Cu^{o} = 0.342$) as compared to Ni^{2+} ($E°$ $Ni^{2+}/Ni^{o} = -0.257$) and Cr^{3+} ($E°$ $Cr^{3+}/Cr^{1+} = -0.744$). Incorporation of a metal ion electron acceptor into the framework or into ion-exchange sites creates a static system in which light energy can be converted into chemical energy and stored for extended periods of time until diffusion of the photoproducts releases it.

Powder ESR spectra (Figure 7) of as-synthesized and calcined CuUHM-3 show Cu(II) species with $A_{||} = 147 \times 10^{-4}$ cm^{-1}. Based on a number of single-crystal ESR studies the $A_{||}$ hyperfine component of Cu(II) gives a guide to its overall coordination symmetry. $A_{||}$ increases from 70×10^{-4} cm^{-1} for tetrahedral coordination, through square pyramidal, octahedral, trigonal bipyramidal to 170×10^{-4} cm^{-1} for square planar coordination.[88] For methanol and acetone adsorbate $A_{||} = 130 \times 10^{-4}$ cm^{-1} seems indicative of distorted octahedral coordination as has also been suggested for water adsorbate.[89] Thus we suggest that Cu(II) is coordinated to four lattice oxgens and two oxygens of adsorbate molecules in a distorted octahedral environment.

The spin Hamiltonian parameters of PC_1/CuUHM-3 (Figure 7) are $g_{||} = 2.3554$, $g_{\perp} = 2.0716$, and $A_{||} = 147 \times 10^{-4}$ cm^{-1} from Cu(II) and $g = 2.0055$ for PC_1^+. The copper ions show that incorporation of the transition metal ion into the framework can change the fraction of the light energy that can be converted into chemical energy.

To study the influence of the metal concentration on the photoyield, several mesoporous CuUHM-3 molecular sieves with different Cu(II) concentrations were prepared. From Figure 8, one can conclude that the photoionization efficiency depends on the metal concentration in ion-exchange sites. It is observed that the photoyield increases as the Cu concentration in the mesoporous UHM-3 molecular sieves decreases. The optimum concentration of Cu(II) in the present study occurs for Cu/Al $= 1 \times 10^{-3}$.

To understand the influence of the alkyl chain length on the photoyield, several mesoporous PC_n/UHM-3 molecular sieves with different n values were prepared. The photoproduced ESR spectra (Figures 9 and 10) for samples containing PC_n ($n > 3$) are similar to the ESR spectrum of PC_3^+ cation radicals in UHM-3 (Si/Al = 2.4). The photoproduced ESR signal in samples containing PC_n is reasonably assigned to photoproduced PC_n^+ cation radicals. The relative mobilities of the PC_n^+ cation radicals are suggested by the breadth and resolution of the ESR spectra in Figures 9 and 10. The broad ESR spectra (PC_n with $n > 1$) indicate that the radicals are largely immobilized at room temperature. The partially resolved ESR spectra with the relative intensities of 1:4:7:7:4:1 (PC_n with $n = 1$) for PC_1^+ cation radical show that PC_1^+ has some mobility in these materials at room temperature. The results suggest a greater mobility for PC_n^+ with smaller alkyl chain length which correlates with greater probability for decay by back electron transfer from UHM-3 or by some other process. The lifetime of the PC_n^+ cation radicals in UHM-3 is a few months at room temperature, depending on the alkyl chain length.

Figures 11 and 12 show a remarkable change in the photoyield of alkylphenothiazine cation radicals with the alkyl chain length. The alkylphenothiazine cation radical photoyield and stability increase from methyl to decyl, and as the alkyl chain length further increases from decyl to hexadecyl the photoyield decreases. A possible explanation for this trend is as follows. When the PC_n alkyl chain length is short, some of the PC_n molecules react with atmospheric oxygen during sample preparation, oxidize, and turn light pink. Increasing the alkyl chain length of the PC_n molecules reduces the extent of this dark reaction with atmospheric oxygen. If the PC_n molecules are distributed uniformly on the surface of UHM-3 independent of alkyl chain length, then the photooxidation yields are expected to increase monotonically. Thus the decreased photooxidation yields for PC_{10}/UHM-3 to PC_{16}/UHM-3 may suggest that PC_{10}/UHM-3 to PC_{16}/UHM-3 are bound nonuniformly on mesoporous UHM-3 molecular sieves which makes oxidation more diffcult.[37,90] In other work, *N*-alkylphenothiazines with longer alkyl chain length are suggested to form clusters and change their reactivity toward oxidizing agents.[91]

The alkyl chain length of PC_n in mesoporous UHM-3 molecular sieves is a critical parameter affecting the yield of photoproducts. This is related to the control of the spatial separation between the electron donor and the acceptor by the alkyl chain length of PC_n. TGA suggests that mesoporous UHM-3 molecular sieves can accommodate molecules such as *N*-alkylphenothiazines inside their channels. The mobility of the molecule depends on its alkyl chain length. Figure 13 shows TGA results obtained from the incorporation of *N*-alkylphenothiazines into UHM-3 samples. All the three curves typically show three weight losses, the first near 50−100 °C is attributed to water desorption, the second near 200 °C (for PC_{16}), 220 °C (for PC_6) or 250 °C (for PC_{10}) is attributed to *N*-alkylphenothiazine desorption, and the third broad peak centered around 470 °C is assigned to the decomposition of *N*-alkylphenothiazines

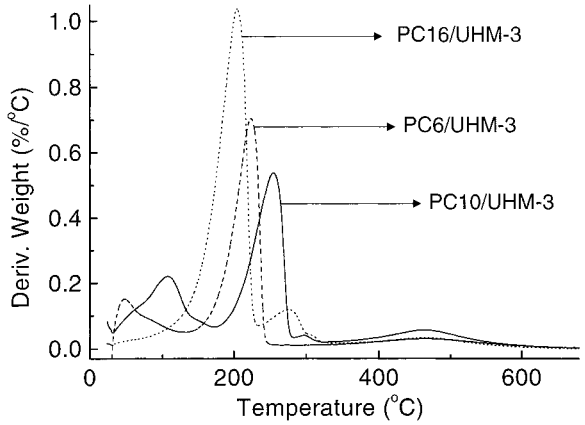

Figure 13. Differential thermal analysis of mesoporous UHM-3 with incorporated hexylphenothiazine, decylphenothiazine, and hexadecylphenothiazine.

in oxygen atmosphere.[55] This decomposition peak is not observed when the experiments are carried out in nitrogen atmosphere. Thus we can conclude from the TGA results that decylphenothiazine (1.4 nm) penetrates mostly into mesoporous UHM-3 (1.7 nm), hexylphenothiazine (1.1 nm) penetrates to a lesser degree into mesoporous UHM-3 molecular sieves, and hexadecylphenothiazine (2.0 nm) penetrates even less into mesoporous UHM-3. This is consistent with the results obtained from the photoionization experiments which show a photoyield decrease in the order, PC_{10}/UHM-3 > PC_6/UHM-3 > PC_{16}/UHM-3.

Conclusions

The *N*-alkylphenothiazine cation radical photoyield and stability in mesoporous transition metal-containing UHM-3 molecular sieves depend on the Si/Al ratio, the nature of the transition metal ion, the metal content, and the alkyl chain length of the PC_n^+ cation radicals. The highest photoyield is obtained for mesoporous copper-substituted UHM-3 molecular sieve as electron acceptor and PC_{10} as electron donor.

Acknowledgment. This research was supported by the Division of Chemical Science, Office of Basic Energy Science, Office of Energy Research, U.S. Department of Energy, by the Texas Advanced Research Program and by the Environmental Institute of Houston.

References and Notes

(1) *Photochemical Conversion and Storage of Solar Energy*; Connolly, J. S., Ed.; Academic: New York, 1981.
(2) *Energy Resources through Photochemistry and Catalysis*; Grätzel, M., Ed.; Academic: New York, 1983.
(3) Kalyanasundaram, K. *Photochemistry in Microheterogeneous Systems*; Academic: New York, 1987.
(4) Grätzel, M. *Heterogeneous Photochemical Electron Transfer*; CRC Press: Boca Raton, FL, 1988.
(5) Fendler, J. H. *Acc. Chem. Res.* **1980**, *13*, 7.
(6) Infelta, P. P.; Grätzel, M.; Fendler, J. H. *J. Am. Chem. Soc.* **1980**, *102*, 1479.
(7) Dewey, T. G.; Hammes, G. G. *Biophys. J.* **1980**, *32*, 1023.
(8) Pileni, M. P. *Chem. Phys. Lett.* **1980**, *71*, 317.
(9) Hurst, J. K.; Lee, L. Y. C.; Grätzel, M. *J. Am. Chem. Soc.* **1983**, *105*, 7048.
(10) Kevan, L. In *Photoinduced Electron Transfer, Part B*; Fox, M. A., Chanon, M., Eds.; Elsevier: Amsterdam, 1988; pp 329−384.
(11) Kevan, L. *Int. Rev. Chem.* **1990**, *9*, 307.
(12) Kevan, L. *Radiat. Phys. Chem.* **1991**, *37*, 629.
(13) Lanot, M. P.; Kevan, L. *J. Phys. Chem.* **1991**, *95*, 10178.
(14) McManus, H. J.; Kang, Y. S.; Kevan, L. *J. Phys. Chem.* **1992**, *96*, 5622.
(15) Kang, Y. S.; McManus, H. J.; Kevan, L. *J. Phys. Chem.* **1993**, *97*, 2027.
(16) Kang, Y. S.; Kevan, L. *J. Phys. Chem.* **1994**, *98*, 4389.
(17) Sung-Suh, H. M.; Kevan, L. *J. Phys. Chem. A* **1997**, *101*, 1414.
(18) Ford, W. E.; Rodgers, M. A. J. *J. Phys. Chem.* **1994**, *98*, 7415.
(19) Ford, W. E.; Rodgers, M. A. J. *J. Phys. Chem.* **1995**, *99*, 5139.
(20) Kurshev, V.; Kevan, L. *Langmuir* **1997**, *13*, 225.
(21) Breck, D. W. *Zeolite Molecular Sieves*; Wiley: New York, 1974.
(22) Slinkin, A. A.; Kucherov, A. V.; Kondrat′ev, D. A.; Bondarenko, T. N.; Rubinshtein, A. M.; Minachev, Kh. M. *J. Mol. Catal.* **1986**, *35*, 97.
(23) Persaud, L.; Bard, A. J.; Campion, A.; Fox, M. A.; Mallouk, T. E.; Webber, S. E.; White, J. M. *J. Am. Chem. Soc.* **1987**, *109*, 7309.
(24) Dutta, P. K.; Incavo, J. A. *J. Phys. Chem.* **1987**, *91*, 4443.
(25) Borja, M.; Dutta, P. K. *Nature* **1993**, *362*, 43.
(26) Ledney, M.; Dutta, P. K. *J. Am. Chem. Soc.* **1995**, *117*, 7687.
(27) McManus, H. J. D.; Finel, C.; Kevan, L. *Radiat. Phys. Chem.* **1995**, *45*, 761.
(28) Vansant, E. F.; Van der Voort, P.; Vrancken, K. C. *Characterization and Chemical Modification of the Silica Surface*; Studies in Surface Science and Catalysis; Elsevier: Amsterdam, 1995; Vol. 93, Chapters 2 and 3.
(29) Scott, R. P. W. *Silica Gel and Bonded Phases*; Wiley: New York, 1993; Chapters 4 and 6.
(30) Bauer, R. K.; Borenstein, R.; De Mayo, P.; Okada, K.; Rafalska, M.; Ware, W. R.; Wu, K. C. *J. Am. Chem. Soc.* **1982**, *104*, 4635.
(31) Slama-Schwok, A.; Ottolenghi, M.; Avnir, D. *Nature* **1992**, *355*, 240.
(32) Marro, M. A. T.; Thomas, J. K. *J. Photochem. Photobiol. A: Chem.* **1993**, *72*, 251.
(33) Wilkinson, F.; Worrall, D. R.; Williams, S. L. *J. Phys. Chem.* **1995**, *99*, 6689.
(34) Xiang, B.; Kevan, L. *Colloid Surf. A* **1993**, *72*, 11.
(35) Xiang, B.; Kevan, L. *Langmuir* **1994**, *10*, 2688.
(36) Xiang, B.; Kevan, L. *J. Phys. Chem.* **1994**, *98*, 5120.
(37) Xiang, B.; Kevan, L. *Langmuir* **1995**, *11*, 860.
(38) Matsuura, K.; Kevan, L. *J. Phys. Chem.* **1996**, *100*, 10652.
(39) Sung-Suh, H. M.; Kevan, L. *J. Chem. Soc., Faraday Trans.* **1998**, *94*, 1417.
(40) Krueger, J. S.; Mayer, J. E.; Mallouk, T. E. *J. Am. Chem. Soc.* **1988**, *110*, 8232.
(41) Slama-Schwok, A.; Avnir, D.; Ottolenghi, M. *Photochem. Photobiol.* **1991**, *54*, 525.
(42) Vermeulen, L. A.; Thompson, M. E. *Nature* **1992**, *358*, 656.
(43) Buck, H. M.; Bloemhoff, W.; Oosterhoff, L. *Tetrahedron Lett.* **1960**, 5.
(44) Forbes, W. F.; Sullivan, P. D. *J. Am. Chem. Soc.* **1966**, *88*, 2862.
(45) Shine, H. J.; Thompson, D. R.; Veneziani, C. *J. Heterocycl. Chem.* **1967**, *4*, 517.
(46) Biehl, E. R.; Chiou, H.; Keepers, J.; Kennard, S.; Reeves, P. C. *J. Heterocycl. Chem.* **1975**, *12*, 397.
(47) Clarke, D.; Gilbert, B. C.; Hanson, P. *J. Chem. Soc., Perkin Trans. 2* **1975**, 1078.
(48) Clarke, D.; Gilbert, B. C.; Hanson, P. *J. Chem. Soc., Perkin Trans. 2* **1976**, 114.
(49) Clarke, D.; Gilbert, B. C.; Hanson, P. *J. Chem. Soc., Perkin Trans. 2* **1978**, 1103.
(50) Fujihara, H.; Fuke, S.; Yoshihara, M.; Maeshima, T. *Chem. Lett.* **1981**, 1271.
(51) Alkaitis, S. A.; Beck, G.; Graetzel, M. *J. Am. Chem. Soc.* **1975**, *97*, 5723.
(52) Moroi, Y.; Braun, A. M.; Graetzel, M. *J. Am. Chem. Soc.* **1979**, *101*, 567.
(53) Kang, Y. S.; Baglioni, P.; McManus, H. J. D.; Kevan, L. *J. Phys. Chem.* **1991**, *95*, 7944.
(54) Hovey, M. C. *J. Am. Chem. Soc.* **1982**, *104*, 4196.
(55) Krishna, R. M.; Prakash, A. M.; Kurshev, V.; Kevan, L. *Phys. Chem. Chem. Phys.* **1999**, *1*, 4119.
(56) Kurshev, V.; Prakash, A. M.; Krishna, R. M.; Kevan, L. *Microporous Mesoporous Mater.* **2000**, *34*, 9.
(57) Kresge, C. T.; Leonowicz, M. E.; Roth, W. J.; Vartuli, J. C.; Beck, J. S. *Nature* **1992**, *359*, 710.
(58) Beck, J. S.; Vartuli, J. C.; Roth, W. J.; Leonowicz, M. E.; Kresge, C. T.; Schmitt, K. D.; Chu, C. T.-W.; Olson, D. H.; Sheppard, E. W.; McCullen, S. B.; Higgins, J. B.; Schlenker, J. L. *J. Am. Chem. Soc.* **1992**, *114*, 10834.
(59) Beck, J. S.; Vartuli, J. C.; Kennedy, G. J.; Kresge, C. T.; Roth, W. J.; Schramm, S. E. *Chem. Mater.* **1994**, *6*, 1816.
(60) Zhao, D.; Luan, Z.; Kevan, L. *J. Chem. Soc., Chem. Commun.* **1997**, 1009.
(61) Zhao, D.; Luan, Z.; Kevan, L. *J. Phys. Chem. B* **1997**, *101*, 6943.
(62) Luan, Z.; Zhao, D.; He, H.; Klinowski, J.; Kevan, L. *J. Phys. Chem. B* **1998**, *102*, 1250.
(63) Luan, Z.; Zhao, D.; Kevan, L. *Microporous Mesoporous Mater.* **1998**, *20*, 93.

(64) Hartmann, M.; Kevan, L. *Chem. Rev.* **1999**, *99*, 635.
(65) Iton, L. E.; Choi I.; Desjardins, J. A.; Maroni, V. A. *Zeolites* **1989**, *9*, 535.
(66) Shiralkar, V. P.; Saldariaga, C. H.; Perez J. O.; Clearfield, A.; Chen, M.; Anthony R. G.; Donohue, J. A. *Zeolites* **1989**, *9*, 474.
(67) Schoonheydt, R. A.; de Vos, R.; Pelgrims, J.; Leeman, H. In *Zeolites, Facts, Figures and Future*; Jacobs, P. A., van Santen, R. A., Eds.; Elsevier: Amsterdam, 1989; p 559.
(68) Gozlan, I.; Ladkani, D.; Halpern, M.; Rabinovitz, M.; Anoir, D. J. *J. Heterocycl. Chem.* **1984**, *21*, 613.
(69) Barrett, E. P.; Joyner, L. G.; Halenda, P. P. *J. Am. Chem. Soc.* **1951**, *73*, 373.
(70) Ravikovitch, P. I.; Wei, D.; Chueh, W. T.; Haller, G. L.; Neimark, A. V. *J. Phys. Chem. B* **1997**, *101*, 3671.
(71) Kruk, M.; Jaroniec, M.; Sayari, A. In *Proceedings of the 12th International Zeolite Conference*; Treacy M. J., Marcus, B. K., Bisher, M. E., Higgins, J., Eds.; Materials Research Society: Warrendale, PA, 1999; p 761.
(72) Lukens, Jr., W. W.; Schmidt-Winkel, P.; Zhao, D.; Feng, J.; Stucky, G. D. *Langmuir* **1999**, *15*, 5403.
(73) Kruk, M.; Jaroniec, M. *Langmuir* **1999**, *15*, 5279.
(74) Oliver, S.; Kuperman, A.; Coombs, N.; Louth, A.; Ozin, G. A. *Nature* **1995**, *378*, 47.
(75) Sayari, A.; Karra, V. R.; Reddy, J. S.; Moudrakovski, J. L. *J. Chem. Soc., Chem. Commun.* **1996**, 411.
(76) Chenite, A.; Page, Y. L.; Karra, V. R.; Sayari, A. *J. Chem. Soc., Chem. Commun.* **1996**, 413.
(77) Sayari, A.; Moudrakovski, J. L.; Reddy, J. S. *Chem. Mater.* **1996**, *8*, 2080.
(78) Sayari, A. In *Progress in Zeolite Microporous Materials*; Chon, H., Ihm, S.-K., Uh, Y. S., Eds.; Studies in Surface Science and Catalysis, Vol. 105; Elsevier: Amsterdam, 1997; p 37.
(79) Gao, Q.; Chen, J.; Xu, E.; Yue, Y. *Chem. Mater.* **1997**, *9*, 457.
(80) Gao, Q.; Chen, J.; Li, S.; Xu, R. In *Progress in Zeolite Microporous Materials*; Chon, H., Ihm, S.-K., Uh, Y. S., Eds.; Studies in Surface Science and Catalysis, Vol. 105; Elsevier: Amsterdam, 1997; p 389.
(81) Cheng, S.; Tzeng, J.-N.; Hsu, B.-Y. *Chem. Mater.* **1997**, *9*, 1788.
(82) Pophal, C.; Schnell, R.; Fuess, H. In *Progress in Zeolite Microporous Materials*; Chon, H., Ihm, S.-K., Uh, Y. S., Eds.; Studies in Surface Science and Catalysis, Vol. 105; Elsevier: Amsterdam, 1997; p 101.
(83) Sing, K. S.; Everett, D. H.; Haul, R. A. W.; Moscow, L.; Pierotti, R. A.; Rouquerol, J.; Siemieniewska, T. *Pure Appl. Chem.* **1985**, *57*, 603.
(84) Lagercrantz, C. *Acta Chem. Scand.* **1961**, *15*, 1545.
(85) Crosignani, E.; Franzosini, P.; Siragusa, G.; Zanotti, L. *Arch. Sci.* **1961**, *24*, 153.
(86) Odiot, S.; Tonnard, F. *J. Chim. Phys.* **1964**, *61*, 382.
(87) Bodea, C.; Silberg, I. *Rev. Roum. Chim.* **1965**, *10*, 887.
(88) Hathaway, B. J.; Billing, D. E.; Dudley, R. J. *J. Chem. Soc. A* **1970**, 1420.
(89) Ichikawa, T.; Yoshida, H.; Kevan, L. *J. Chem. Phys.* **1981**, *75*, 2485.
(90) Louis, L.; Tozer, T. N.; Tuck, L. D.; Loveland, D. B. *J. Med. Chem.* **1972**, *15*, 898.
(91) Pelizzetti, E.; Mentasi, E. *Inorg. Chem.* **1979**, *18*, 583.